COBEM 2021 26th International Congress of Mechanical Engineering
November 22-26, 2021, Virtual Congress, Brazil

COB-2021-XXXX
IMPROVED PRELIMINARY GEOMETRY FOR SCO_2 CENTRIFUGAL COMPRESSORS THROUGH FULL 1D MODELING

Gustavo Singulane Gonçalves
Elóy E. Gasparin
Vitor Cesar N. Mattos
Bruno Barbizan
São Paulo State University, Ilha Solteira, 15385-000, SP, Brazil
gustavosingulane@gmail.com
eloygasparin@gmail.com
vitormattosn@gmail.com
bruno.barbizan@unesp.br

Paulo Eduardo B. Mello
Educational Foundation of Ignatius Father Sabóia de Medeiros, São Bernardo do Campo, 09850-901, SP, Brazil
pmello@fei.edu.br

Fábio Saltara
University of São Paulo, São Paulo, 05508-580, SP, Brazil
fsaltara@usp.br

Daniel J. Dezan
Federal University of ABC, Santo André, 09210-580, SP, Brazil
daniel.dezan@ufabc.edu.br

Jurandir I. Yanagihara
University of São Paulo, São Paulo, 05508-580, SP, Brazil
jiy@usp.br

Leandro O. Salviano
São Paulo State University, Ilha Solteira, 15385-000, SP, Brazil
leandro.salviano@unesp.br

Abstract. *In order to extend the life of oil deposits, and therefore the profit from them, a technique called Enhanced Oil Recovery (EOR) can be used. One of the methods for performing this technique is the reinjection of CO_2 in the oil reservoir, which not only increases the oilfield life, but also provides a way to permanently sequester carbon dioxide. To accomplish the high pressures required for the reinjection at such depths, supercritical CO_2 compressors must be developed. The numerical analysis of the thermal-hydraulic behavior of this equipment usually requires complex and high computational cost for 3D simulations. In order to provide faster and reliable results, a code for the full compressor was written in Python programming language, being an open-source alternative to obtain preliminary results that can provide a starting point for the centrifugal compressor geometry for a 3D design. For a full 1D modeling, a supercritical CO_2 centrifugal compressor with impeller, vaneless diffuser and volute is considered. The available 1D models in the literature related to geometry and losses were studied and implemented under hypothesis: steady state, vaneless diffuser, constant passage width in the diffuser, constant angle between tangential, meridional and absolute velocities throughout the diffuser and incompressible flow in the volute. Eight geometrical parameters are submitted to a screening sensitivity analysis method using the 1D model and their impact towards isentropic efficiency, power required and pressure recovery are assessed. A 3D compressor model consisting in impeller and diffuser is simulated, assuming steady state flow, SST k-omega turbulence model and Span and Wagner equation of state. An improved 3D geometry is created based on insight obtained from Morris' sensitivity analysis method, 1D and 3D evaluations. The 1D model is validated through experimental data and 3D model is used for better understanding of physical phenomena differences between original and improved designs. This methodology can significantly increase the machine performance using relatively low computational resources.*

Keywords: *centrifugal compressor, CFD, one-dimensional model, loss models.*

1. INTRODUCTION

The oil industry provides resources for the manufacturing of a variety of products that are strongly present in human life, from plastics to fuels, oil finds its way even in clothing articles with petroleum-based fibers. Due to the importance of oil in the world's economy, improving the efficiency of its extraction is of great interest, not just to increase profits, but to expand the life of the non-renewable reservoirs while there is no alternative for oil-based products (McLeroy et al., 2019). In common oil extraction processes, part of the oil remains attached to the rock pores in the reservoir, which implies in a loss of oil along the extraction with a premature end to the oil field life due to the lack of a method to collect the remaining resources. In order to increase the field life and capture the remaining oil an enhanced oil recovery technique (EOR) can be used. This method uses the injection of a solvent in the oil field as a way to "drag" any oil stuck in the rock pores out of them, enabling its extraction (NETL, 2010). Many substances could be mixed with the oil for this technique, but due to its low-price CO_2 is commonly used, working not just as a way to grab the oil, but also to create a mix that is less viscous than the pure oil, helping with the extraction. The EOR technique also provides an environmental interest because it is a way to permanently sequester CO_2, since part of the gas gets trapped in the rock pores and even the gas that is collected with the oil is then separated and reinjected in the process (NETL, 2010).

In order to achieve CO_2 injection in the depths of the oil reservoir, the gas must be highly pressurized, reaching its supercritical state, which creates the need for a design of a SCO_2 compressor (Khan et al., 2013). Developing a compressor for this application requires a numerical analysis of the thermal and hydraulic behavior of the turbomachine, which usually means a high computational cost in 3D simulations using CFD software. In order to decrease the computational cost and provide a preliminary analysis and a starting design for the compressor, this paper presents a 1D model for a SCO_2 centrifugal compressor along with its validation and sensitivity analysis, followed by an CFD phenomenological study.

2. METHODOLOGY

The SCO_2 centrifugal compressor model presented in this study can be separated in three main components: impeller, vaneless diffuser and volute. Figure (1) displays the compressor components, as well as the nomenclature used for each of their inlets and outlets.

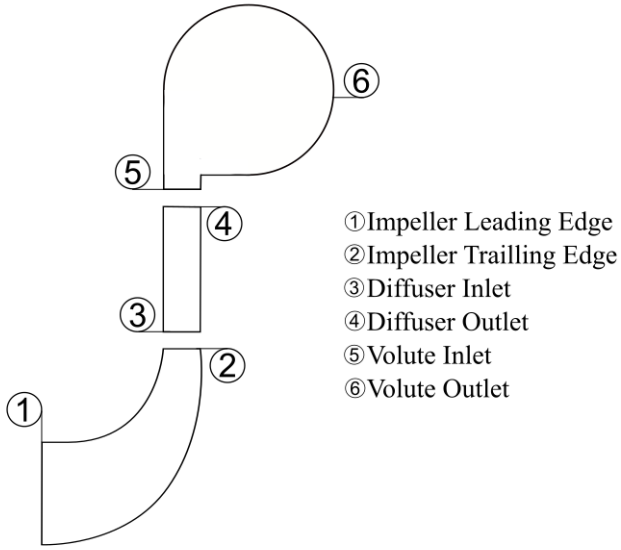

Figure 1. Compressor 1D model and nomenclature.

The specific speed (N_s) and the specific diameter (D_s) for the compressor are chosen based on the definitions made in Balje (1981) and have values of 0.3 and 7.5 respectively.

2.1 Impeller Model

The compressor analysis starts at the impeller with a calculation for the minimum inlet hub radius ($r_{1h,min}$) that ensures the safe operation of the shaft based on the torque transmitted to the shaft (T) and a pure torque loading (Loewenthal, 1984).

$$r_{1h,min} = \left(\frac{2T}{\pi(0.7\tau_{yield})}\right)^{1/3}, \quad (1)$$

$$T = 9550\frac{\dot{W}_p}{n}, \quad (2)$$

where τ_{yield} is the yield strength of 13Cr-4Ni (UNS S42400) Stainless steel, $\dot{W}_p$ is the transmitting shaft power (kPa) and n is the rotational speed (rpm). The real inlet hub radius is chosen with a 1.2 safety factor based on the minimum radius calculated.

2.1.1 Impeller Leading Edge

The impeller leading edge analysis is made in order to obtain the velocity triangles at incidence and throat along with the leading-edge blade angles. The assumption of $C_{1,U} = 0$, along with the incidence flow area (A_1) and the tangential velocity (U_1) will be used to define the leading edge in an iterative procedure.

$$A_1 = \pi\left(r_{1s}{}^2 - \pi(r_{1h}{}^2)\right) - (r_{1s} - r_{1h})t_1 Z_{fb} \quad (3)$$

$$\mathrm{U}_{1,s} = \omega \mathrm{r}_{1s}, \quad (4)$$

where Z_{fb} is the number of blades, t is the blade thickness and ω is the rotational speed (rad/s).

With the previous calculous done, the iterative process that defines the leading edge can begin, considering the thermodynamic state of the inlet as an initial guess for the leading-edge state (Brenes, 2014a). The iteration loop goes as follows: Absolute velocity (C_1) is determined through mass conservation:

$$C_1 = \frac{\dot{m}}{\rho A_1}, \quad (5)$$

followed by the static enthalpy (H_1) determination by energy conservation and then the calculation of static pressure (P_1):

$$\mathrm{H}_1 = \mathrm{H}_{\mathrm{in}} - \frac{\mathrm{C}_1{}^2}{2}, \quad (6)$$

$$P_1 = P_{in} - \rho_1 \frac{C_1{}^2}{2}, \quad (7)$$

Now, the thermodynamic state can be obtained by an equation of state (R.Span and W.Wagner 1994) as a function of H_1 and P_1, and the convergence can be verified by the value of C_1. After the absolute velocity converges the incidence angle (β_1) cand be analyzed.

$$\beta_1 = tan^{-1}\left(\frac{U_1}{C_1}\right), \quad (8)$$

This procedure is done at the hub and shroud radius as well as at the mid-position radius. Once the incidence angles for the three radii are analyzed the leading-edge incidence geometry is completely determined. In an analog method, the compressor throat also needs to be evaluated, since its higher Mach numbers can cause shockwaves or even condensation of the fluid (Brenes et al., 2014b). The only differences of the throat iterative solution is that the preliminary guess for its thermodynamic state is the previously assessed leading-edge state and that the throat velocity (C_{th}) has to be decomposed in its tangential and meridional components. When C_{th} converges, the throat Mach number is calculated and if it indicates the occurrence of condensation or shockwaves the process must be restarted with changes in the starting parameters. Upon reaching said convergence, the leading-edge losses can be calculated (Aungier, 2000), these losses consist in a sudden contraction loss ($\bar{\omega}_{\mathrm{cont}}$) (Brenes, 2014a) and other losses as: incidence loss ($\bar{\omega}_{inc}$), diffusion loss ($\bar{\omega}_{DIF}$) and, if sonic flow is reached in the throat, choking loss ($\bar{\omega}_{CH}$). These losses are shown from Eq. (9) to Eq. (12).

$$\bar{\omega}_{cont} = \frac{r_{1h}{}^4}{r_{1s}{}^4}, \quad (9)$$

$$\bar{\omega}_{\mathrm{inc}} = 0.8\left(1 - \frac{\mathrm{C}_{1,\mathrm{m}}}{\mathrm{w}_1\cos(\beta_1)}\right)^2 + \left(\frac{\mathrm{Z}_{\mathrm{fb}}\mathrm{t}_1}{2\pi \mathrm{r}_1\cos(\beta_1)}\right)^2, \quad (10)$$

$$\bar{\omega}_{DIF} = 0.8\left(1 - \frac{w_{th}}{w_1}\right)^2 - \bar{\omega}_{inc}, \tag{11}$$

$$\begin{aligned} &\bar{\omega}_{\mathrm{CH}} = 0.5(0.05\mathrm{X} + \mathrm{X}^7), \text{ if } \mathrm{X} > 0, \\ &\bar{\omega}_{CH} = 0, if\ X \leq 0, \end{aligned} \tag{12}$$

where X is calculated as follows, along with the contraction ratio correlation (C_r) and the sonic throat area (A^*).

$$\begin{aligned} &X = 11 - 10C_r A_{th}/A^*, \\ &C_r = \sqrt{A_1 \cos(\beta_1)/A_{th}}, \\ &A^* = \frac{\dot{m}}{\rho_{th} a_{th}}, \end{aligned} \tag{13}$$

With the sum of the losses, a corrected thermodynamic state for the throat is calculated iteratively by energy conservation and pressure loss, once this state reaches convergence, the leading edge is fully finished.

The presence of condensation in the throat is checked through the comparison of C_{th} with the fluid Acceleration Margin to Condensation (AMC) (Brenes, 2014a), that indicates the maximum allowed Mach number at the impeller throat to avoid such phenomenon. The AMC is calculated as follows:

$$\begin{aligned} &AMC = \frac{v_{sat}}{a_{sat}}, \\ &s_{sat} = s_{in}, \\ &v_{sat} = \left(2(h_{in} - h_{sat})\right)^{1/2}, \end{aligned} \tag{14}$$

where v_{sat} is the maximum velocity to avoid condensation, h_{in} and s_{in}, are the enthalpy and entropy at the compressor inlet, h_{sat} and s_{sat} are enthalpy and entropy of an isentropic process at saturation and a_{sat} the sound velocity at the saturation line.

2.1.2 Impeller Trailing Edge

For the impeller trailing edge analysis, an initial guess for the losses of the diffuser and volute ($K_{dif-vol}$) and the total-to-total isentropic efficiency of the impeller ($\eta_{s,tt}$) and it is considered that the trailing edge will compensate these losses by a rise in total pressure. The initial guesses for the previous parameter are of 10% and 80% respectively, for the first iteration an ideal performance is considered, where the distortion factor (λ) and the slip factor (σ) have unitary value and the losses between impeller inlet and outlet are inexistent (Brenes, 2014a). With these considerations the first loop of the trailing edge is initiated by an estimation of its thermodynamic state and by determining, trough Euler's equation, the tangential and meridional absolute velocities at the trailing edge ($C_{U,2}$ and $C_{m,2}$).

$$\begin{aligned} &P_{t,2} = \frac{P_{t,6}}{1 - K_{dif-vol}}, \\ &h_{t,2} = h_{t,1} + \frac{\Delta h_{t,s}}{\eta_{s,tt}}, \end{aligned} \tag{14}$$

$$\begin{aligned} &C_{U,2} = \frac{h_{t,2} - h_{t,1}}{U_2} + \frac{r_1}{r_2} C_{U,1}, \\ &C_{m,2} = \sigma C_{m,1}, \end{aligned} \tag{15}$$

Now, a middle loop begins, in order to calculate the trailing edge blade height and the impeller losses. However, before these calculations, an inner loop must be done, this loop begins by calculating the trailing edge blade angle (β_2) and its thermodynamic state, then the fluid static thermodynamic conditions and specific density are updated. The inner loop ends by calculating the trailing edge absolute velocity (C_2) and is repeated until this velocity reaches convergence.

.

$$\beta_2 = tan^{-1}\left(\frac{U_2 - \frac{C_{U,2}}{\sigma}}{\lambda C_{m,2}}\right), \tag{16}$$

$$
\begin{aligned}
&\mathrm{C}_2 = \left(\left(\lambda \mathrm{C}_{\mathrm{m},2}\right)^2 + \left(\frac{\mathrm{C}_{\mathrm{U},2}}{\sigma}\right)^2\right)^{1/2}, \\
&h_2 = h_{t,2} - \frac{{C_2}^2}{2}, \\
&P_2 = P_{t,2} - \rho_2 \frac{{C_2}^2}{2},
\end{aligned} \tag{17}
$$

Coming back to the middle loop, the blade height (b_2) is calculated by continuity followed by the update of its losses. The middle loop ends with the convergence of b_2 and, once it ends, the isentropic efficiency is updated and the first loop is repeated until its convergence.

$$
b_2 = \frac{\dot{m}}{2\rho_2 \lambda C_{m,2}\left(\pi r_2 - Z_{fb} t_2\right)}, \tag{18}
$$

2.1.3 Impeller Losses

The impeller presents the main losses in the compressor, the loss models utilized were based on what is presented in Aungier (2000), with the use a friction coefficient (C_f) from Schlichting (1979) for the friction loss. The losses defined in the model are: friction loss ($\bar{\omega}_{fr}$), blade-to-blade loading loss ($\bar{\omega}_{BL}$), hub-to-shroud loading loss ($\bar{\omega}_{HS}$), distortion loss ($\bar{w}_{\lambda}$), wake mixing loss ($\bar{\omega}_{wake}$), clearance gap loss ($\bar{\omega}_{CL}$).

$$
\begin{aligned}
&\bar{\omega}_{fr} = 4C_f \frac{L_B}{\bar{d}_H}\left(\frac{\bar{w}}{w_1}\right)^2, \\
&L_B = \frac{\pi}{8}\left(2r_2 - 2r_1 - b_2 + 2\Delta Z\right)\left(\frac{4}{cos\beta_{1s} + cos\beta_{1h} + 2cos\beta_2}\right), \\
&\bar{w} = \sqrt{\frac{\left(w_1^2 + w_2^2\right)}{2}}, \\
&\Delta Z = r_2 * \left(0.014 + 0.023 * \left(\frac{r_2}{r_{1h}}\right) + 1.58\varphi\right),
\end{aligned} \tag{19}
$$

where L_b is the impeller channel length (Ameli et al., 2019), d_H is the meand hydraulic diameter (throat and trailing edge), $\bar{w}$ is the mean relative velocity at the impeller and ΔZ is the axial length.

$$
\begin{aligned}
&\bar{\omega}_{Bl} = \frac{1}{24}\left(\frac{\Delta w}{w_1}\right)^2, \\
&\Delta w = \frac{2\pi d_2 U_2 I_B}{Z_{eff} L_B}, \\
&Z_{eff} = Z_{FB} + Z_{SB}\left(\frac{L_{SB}}{L_{FB}}\right), \\
&L_{SB} = L_{SF} L_{FB}, \\
&I_B = \sigma\left(1 - \frac{\dot{m}\,\lambda \tan\beta_2}{\rho_2 A_2 U_2}\right) - \frac{U_1 C_{U1}}{{U_2}^2},
\end{aligned} \tag{20}
$$

where Δw is the maximum velocity difference, Z_{eff} is the effective number of blades, L_{SF} is the ratio between the size of the splitter blade and full blade, and I_B is the work input coefficient with a slip factor (σ) obtained as in Wiesner (1967)

$$
\begin{aligned}
&\bar{\omega}_{HS} = \frac{1}{6}\left(\frac{\bar{k}_m\,\bar{b}\,\bar{w}}{w_1}\right)^2, \\
&\bar{k}_m = \frac{\alpha_{C1} - \alpha_{C2}}{L_B}, \\
&\bar{b} = \frac{\left(r_{1s} - r_{1h}\right) + b_2}{2}, \\
&\bar{w} = \frac{w_1 + w_2}{2},
\end{aligned} \tag{21}
$$

in which $\bar{k}_m$ is the stream line curvature, $\bar{b}$ is the mean channel width and $\bar{w}$ is the mean relative velocity at the impeller.

$$\begin{aligned}
&\overline{\omega}_{\lambda} = \left(\frac{(\lambda-1)C_{m2}}{w_1}\right)^2, \\
&\lambda = \frac{1}{1-B_2}, \\
&B_2 = \overline{\omega}_{fr}\frac{P_{t,1}-P_1}{P_{t,2}-P_2}\sqrt{\frac{w_1\bar{d}_H}{w_2 b_2}} + \left(0.3+\frac{b_2^2}{L_B^2}\right)\frac{A_R^2\rho_2 b_2}{\rho_1 L_B} + \frac{\delta_{CL}}{2b_2}, \\
&A_R = \frac{A_2 cos\beta_2}{A_1 cos\beta_{th}},
\end{aligned} \tag{22}$$

$$\overline{\omega}_{wake} = \left(\frac{C_{m2,wake}-C_{m2,mix}}{w_1}\right)^2, \tag{23}$$

in which λ is the distortion factor, B_2 is the blockage and δ_{CL} is the clearance gap size.

$$\begin{aligned}
&\overline{\omega}_{CL} = \frac{2\,\dot{m}_{CL}\Delta P_{CL}}{\dot{m}\,\rho_1 w_1^2}, \\
&\dot{m}_{CL} = \rho_2\, Z_{eff} s L_B C_{CL}, \\
&\Delta P_{CL} = \frac{\dot{m}\left(r_2 C_{U,2} - r_1 C_{U,1}\right)}{Z_{eff}\,\overline{r}\,\overline{b} L_B}, \\
&C_{CL} = 0.816\sqrt{2\Delta P_{CL}/\rho_2},
\end{aligned} \tag{24}$$

where $\dot{m}_{CL}$ is the clearance gap mass flow, ΔP_{CL} is the pressure difference between the blade sides and C_{CL} is the clearance absolute velocity.

The total pressure at the impeller must be analyzed in a rotating frame of reference and only after this analysis that the absolute state can be corrected and the total-to-total isentropic efficiency can be updated until convergence, putting an end to the impeller trailing edge calculations.

2.2 Vaneless Diffuser and Volute Model

The diffuser and volute models were implemented to improve the estimation of its total pressure losses, and with it, get an improvement in the impeller analysis, they were based in the considerations presented in the studies of Aungier (2000), Brenes (2014a) with loss models recommended by Oh et al. (1997). The diffuser was modelled with the following considerations: vaneless, diffuser inlet blade height (b_3) is equal to the impeller outlet blade height (b_2), diffuser inlet thermodynamic state is equal as the impeller trailing edge state and a constant angle between tangential, meridional and absolute components in the diffuser.

The diffuser loop is fairly simple, consisting in increments in the diffuser radius until a convergence of its exit static pressure (P_4) is reached. On the start of each iteration the boundary layer thickness (δ) and fractional area blockage (B) are calculated, then, the thermodynamic state is evaluated with a proper equation of state (R.Span and W.Wagner 1994) and the meridional and absolute velocities at the diffuser outlet are obtained through momentum and mass conservation. The velocities are calculated in an inner loop, in order to obtain a converging specific density, similarly to what have been done in the impeller model.

$$\begin{aligned}
&\delta = \frac{b_2}{2}\left(1-\left(\frac{b_2}{r_4}\right)^{0.15}\right), \\
&B = \frac{\delta}{4b_2},
\end{aligned} \tag{15}$$

$$\begin{aligned}
&C_{m,4} = \frac{\dot{m}}{2\pi r_4 b_2 \rho_4 (1-B)}, \\
&C_{u,4} = C_{u,3}\left(\frac{r_3}{r_4}\right),
\end{aligned} \tag{26}$$

With the diffuser entry and exit states defined, the vaneless diffuser enthalpy can be calculated according to Stanitz (1952)

$$\Delta h_{diff} = C_p T_{t,3} \left(\left(\frac{P_4}{P_{t,4}} \right)^{\frac{\gamma-1}{\gamma}} - \left(\frac{P_4}{P_{t,3}} \right)^{\frac{\gamma-1}{\gamma}} \right), \tag{27}$$

The enthalpy loss is then used to update the diffuser exit total pressure ($P_{t,4}$) and, when the exit static pressure converges the diffuser total pressure loss coefficient (K_{diff}) can be computed.

$$K_{dif} = 1 - \frac{P_{t,4}}{P_{t,3}}, \tag{28}$$

With the diffuser defined, the volute analysis begins and its inlet thermodynamic state and velocities are considered to be the same as the diffuser outlet state. As it is discussed in Aungier (2000) and Brenes (2014a) there is very little variation in the fluid specific density at the volute, therefore the fluid compressibility is not taken in consideration in the volute, especially since the one-dimensional analysis is already an approximation for the three-dimensional flow in turbomachines. The volute is considered to be circular and its geometry is solved based on a sizing parameter (*SP*) that is settled as a target for the iterative process. In each iteration, the volute exit radio is incremented and after obtaining its outlet area (A_6) its absolute velocity (C_6) is evaluated through mass conservation.

$$\begin{aligned} A_6 &= \pi (r_6 - r_5)^2, \\ C_6 &= \frac{\dot{m}}{(\rho_6 A_6)}, \end{aligned} \tag{29}$$

The volute losses occur due to a change in meridional velocity ($\overline{w}_m$), loss of angular momentum ($\overline{w}_U$) and due to friction ($\overline{w}_{fr,v}$). The volute hydraulic diameter ($d_{H,v}$) and characteristic length (L_v)

$$\begin{aligned} \overline{w}_m &= \left(\frac{C_{m,5}}{C_5} \right)^2, \\ \overline{w}_U &= \frac{1}{2} \frac{r_5 {C_{U,5}}^2}{r_6 {C_5}^2} \left(1 - \frac{1}{SP} \right), \\ \overline{w}_{fr,v} &= 4 c_f \left(\frac{C_6}{C_5} \right)^2 \frac{L_v}{d_{H,v}}, \\ L_v &= \pi \frac{r_5 + r_6}{2}, \\ d_{H,v} &= \frac{4 A_6}{\pi}, \end{aligned} \tag{30}$$

With the losses computed, the sizing parameter is analyzed and the loop is repeated until SP reaches the targeted value. Then the volute total pressure is calculated and its total pressure loss coefficient (K_{vol}) is obtained.

$$SP = \frac{r_5 C_{U,5}}{r_6 C_{U,6}}, \tag{31}$$

$$\begin{aligned} P_{t,6} &= P_{t,5} - (P_{t,5} - P_5) \sum_5^6 \overline{\omega}_i, \\ K_{vol} &= 1 - \frac{P_{t,6}}{P_{t,5}}, \end{aligned} \tag{32}$$

2.3 Model Validation

The 1D model presented was validated with the results from the test 'CBC_081202_1003' recorded in the Sandia report (Wright et al., 2010). The outlet total pressure (P_{t6}) from the tests was compared with the 1D results obtained when the model geometry and operational inputs were settled as the Sandia tests parameters. Table (1) shows the comparison between the tests and the one-dimensional model.

As seen in the Table (1), all comparisons presented errors below 2%, along with the fact that this is a 1D preliminary analysis, the results obtained shows the good agreement of the described model with experimental data.

Table 1. Comparison between test CBC_081202_1003 and the 1D model.

n [rpm]	$\dot{m}$ [kg/s]	T_{in} [K]	P_{in} [MPa]	PR	P_{t6} Exp.	P_{t6} 1D	Error (%)
55000	3.969	304.4	7.722	1.18	9.101	9.273	1.89%
55000	3.719	304.4	8.067	1.26	10.135	10.283	1.46%
55000	3.402	304.4	8.136	1.31	10.687	10.794	1.00%
55000	2.540	304.4	8.170	1.42	11.583	11.683	0.86%
55000	1.670	304.4	8.205	1.47	12.066	12.104	0.31%

The Sandia reports also have experimental values for pressure ratios (PR) below 1.18, however such low PR values don't represent the situation of the compressor presented in this paper. The low mass flow of the experimental tests isn't the best for the evaluation of a compressor intended for the enhanced oil recovery, but due to the lack of other experimental data the Sandia tests present a good initial validation.

In order to complement the validation obtained through the Sandia Report, a 3D CFD model was built as a way to verify physical phenomena at the geometry defined by the one-dimensional analysis, making the model more robust.

2.4 Sensitivity analysis

A sensitivity analysis for the one-dimensional model was made by the elementary effects method devised by Morris (1991) in order to define the effects of the inputs towards the outputs and identify possible interactions between the factors analyzed (Saltelli, 2008) (Ge, 2014). For this analysis, eight inputs and three outputs were chosen as follows: Inputs: number of blades (Z_{fb}),splitter length ratio (L_{sf}), pressure ratio (PR), impeller axial length (ΔZ), volute target sizing parameter (SP_{target}), r_{1s}, t and b_4; Outputs: Pressure Recovery (c_P), Required Power (W_{rec}) and Isentropic Efficiency ($\eta_{s,tt}$). The outputs were chosen in order to represent the main parameters of the compressor performance that are calculated in the presented model. In order to conduct the sensitivity analysis, the input ranges were defined based on the space sample region where the model realizations did not fail or were unfeasible, and are presented in Table (2).

Table 2. Inputs range for the sensitivity analysis.

Parameters	Range	
	Min.	Max.
L_{sf}	0.43	0.9
PR	3.3	3.8
SP_{targ}	1.1	1.8
Z_{fb}	6	12
b_4 [m]	0.003	0.008
ΔZ [m]	0.01	0.05
r_{1s} [m]	0.0428	0.045
t [m]	0.002	0.0027

The sensitivity measures analyzed were the absolute average of the EE distribution (μ^*) (Campolongo et al., 2007) and the deviation of each input EE distribution (σ). In order to determine if a variable is influential or non-influential and important or unimportant, a threshold (value of μ^* that account for 80% of output variation) and a line representing the standard error of the mean ($\mu^* = 2SEM_i$) is established (Vanrolleghem, 2015). The variable classification and identification are done as follows: non-influential variables are located before the threshold, interacting variables are seen above the $\mu^* = 2SEM_i$ line and the important variables are located below said line.

2.5 Three-dimensional model

In order to begin the 3D simulation a geometric model of the compressor must be made, having as a starting point the outputs of the 1D code and the project parameters. These inputs are inserted in Ansys BladeGen in order to generate the blade geometry needed to proceed, this geometry is then sent to TurboGrid where the computational mesh is generated and manually adjusted, both to remove any errors and to establish the element count.

After the computational mesh is done, the final setup for the simulation can begin, the analysis is done in a symmetric domain that consists in a radial cut of the compressor containing a full blade and a splitter, with mass conservation between the meridional surfaces of the domain. The calculations for the gas properties are done though an RGP table with a

resolution of 0.1 MPa and 0.5 K. The blade geometry and simulation domain are illustrated in Figure (2) and the mesh limits are shown in Table (3).

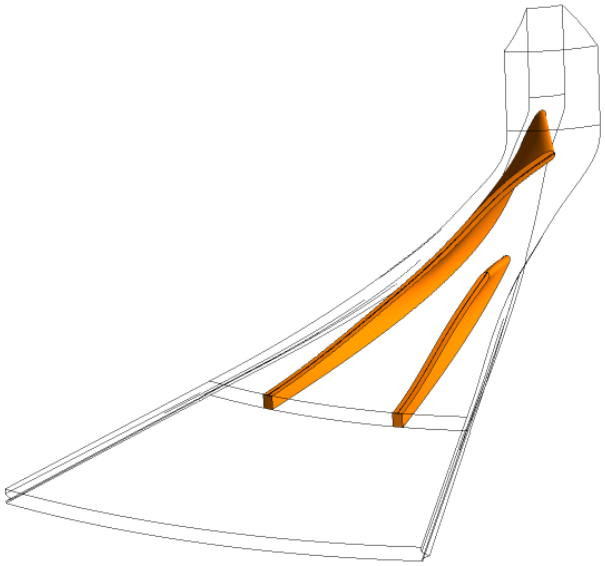

Figure 2. Blade and splitter in the simulation domain.

Table 3. Mesh Limits.

Parameter	Value
Minimum Face Angle [°]	15
Maximum Face Angle [°]	165
Maximum Element Volume Ratio	20
Minimum Volume [m³]	0
Maximum Edge Length Ratio	1000
Maximum Connectivity Number	12

2.6 Design improvement

Initially, a baseline model was established in order to provide a mean of comparison between new geometries. This model was based in the compressor characteristics available in literature, mainly in what's contained in Aungier (2000). After a baseline model was established the 1D code was utilized in order to reach a better design, for that, the most important inputs (identified by the previous sensibility analysis) were changed one by one in a way to reach higher values of isentropic efficiency, these inputs could only be tested independently because the sensitivity analysis showed that there was no interaction between them (Figure 4). With this new geometry at hand, a 3D simulation was done and its results were compared to the ones expected by the 1D analysis, usually there is a divergency in the results, mainly in the pressure ratio (PR) reached by the compressor. In order to reach the final improved geometry a calibration process is done for both the baseline and improved geometry, using the 3D pressure ratio as a feedback to the 1D code until both models reach similar ratios. This calibration is done with small changes in the compressor specific diameter (D_s) and speed (N_s), such changes are done manually and due to the dependence of 3D results this final process can take some time. Once this process is done, the improved geometry is reached and can be analyzed. A flowchart of the design improvement procedure is shown in Figure (3).

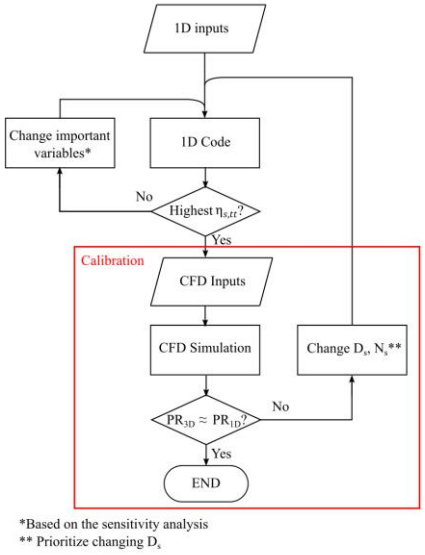

Figure 3. Design improvement flowchart

3. RESULTS

3.1 Sensitivity analysis

Figures (4) through (6) show the main effects sensitivity measures and the analysis of its interactions for the three chosen output parameters.

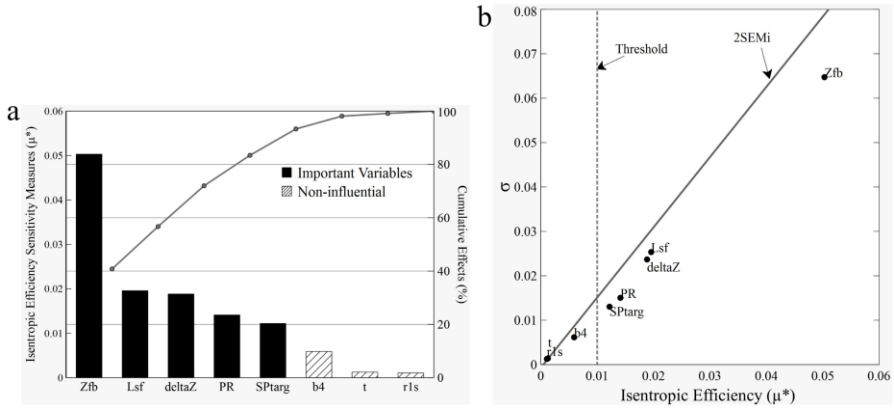

Figure 4. Main effects sensitivity measures (a) and interaction effects analysis (b) of the Morris screening method for the Isentropic Efficiency.

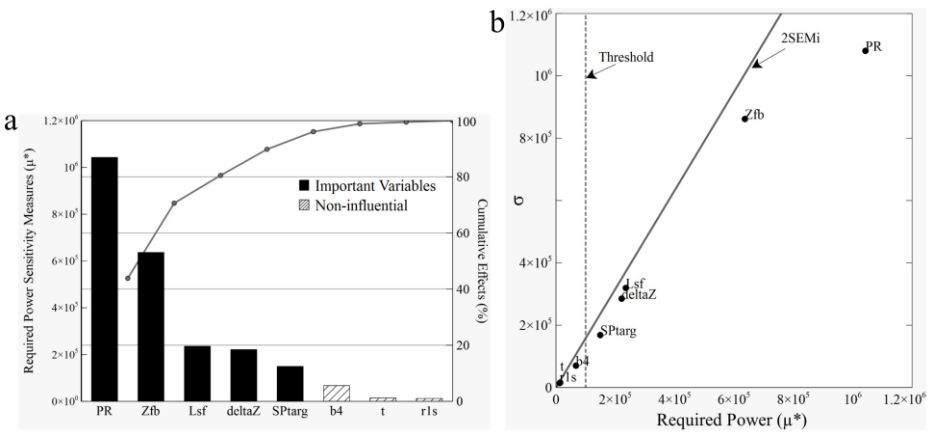

Figure 5. Main effects sensitivity measures (a) and interaction effects analysis (b) of the Morris screening method for the Required Power.

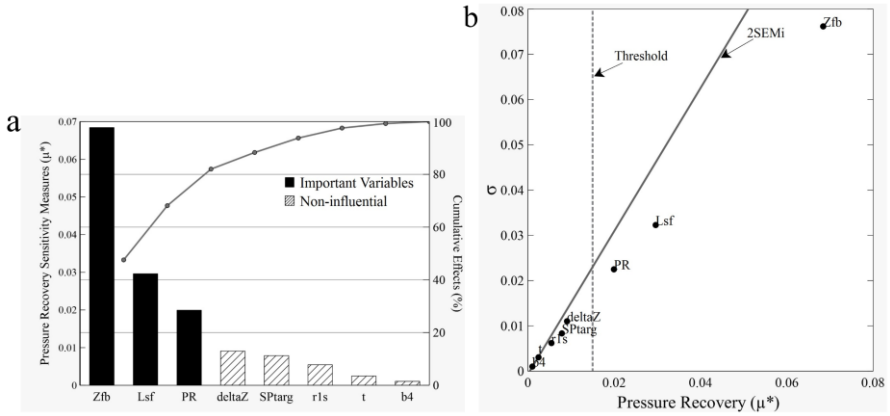

Figure 6. Main effects sensitivity measures (a) and interaction effects analysis (b) of the Morris screening method for the Pressure Recovery coefficient.

The sensitivity analysis shows that the inputs b_4, t and r_{1s} are characterized as non-influential to all the outputs, this classification happens due to the low ranges of these variables in the space sample which was limited by the model feasibility, i. e., the present analysis was made with the higher ranges that allowed the code to function properly, without errors, so the low ranges for these variables were required in the process.

The analysis shows high effects of the number of full blades (Z_{fb}), splitter length (L_{sf}) and pressure ratio (PR) in all the output parameters, indicating the importance of such variables in determining an improved design geometry. The Morris screening method also shows that there is no interaction between the variables, which can be seen due to the fact that they are all below the $2SEM_i$ line. This allows the improvement procedure to be done manually, since each input variable is changed one-at-a-time and the higher isentropic efficiency is chosen after all.

3.2 Improvement procedure analysis

Based on the results obtained by the sensitivity analysis the number of blades (Z_{fb}), splitter length ratio (L_{sf}) and pressure ratio (PR) were changed in the 1D model to obtain an improved geometry, the volute sizing factor (SP_{targ}) wasn't considered because the volute isn't available in the CFD model. It is important to know that since the pressure ratio is changing, the inlet pressure is also changing in order to maintain the outlet pressure required by the project.

The values of the baseline geometry, as well as the ones obtained for the optimized one provided by the 1D model are presented in Table (4).

Table 4. Baseline and improved geometries

Parameters	Baseline	Improved
Pressure Ratio	3.4	3.8
Inlet pressure [MPa]	7.5	6.75
Rotational Speed [rpm]	19640	21600
Inlet hub radius [mm]	16.9	17.5
Inlet shroud radius [mm]	44.0	46.0
Outlet radius [mm]	130.8	125
Outlet blade height [mm]	3.65	5
Impeller axial length [mm]	36.0	36
Number of blades/splitters	12	12
Beta,hub [°]	31.4	31.3
Beta,mid [°]	47.7	47.8
Beta,shroud [°]	57.8	58
Beta Trailing Edge [°]	-1.6	-1.43
Diffuser Radius [mm]	211.9	195
Diffuser Pressure Recovery	0.56	0.53
Isentropic Efficiency [%]	83.59	84.25
Required power [MW]	3.34	4.02

Both the baseline and optimized geometry were simulated through CFD with a coarse mesh of 700 thousand elements. The results obtained for the compressor isentropic efficiency and required power, along with the most impactable variables are shown in Table (5).

Table 5. Baseline and improved results.

Variables	Baseline CFD Model	Improved CFD Model
Number of Blades	12	12
Splitter Length Ratio	0.7	0.9
Pressure Ratio	3.4	3.8
Diffuser Pressure Recovery	0.48	0.48
Isentropic Efficiency [%]	79.27%	81.28%
Required power [MW]	3.82 MW	4.3 MW

The results show an increase in 2.01% in the compressor isentropic efficiency due to the changes obtained from the one-dimensional analysis, proving the methods effectiveness. Along with the increase in efficiency, the results show that the compressor pressure ratio should increase, this proves to be interesting especially in compressor trains, since this allows for smaller ratios in previous compressors. However, further studies need to be done in order to determine how to increase the efficiency in a full compressor train, since a higher local efficiency doesn't necessarily mean a higher efficiency in the full train. It's important to highlight that the number of blades remained the same because it reached its higher bound of 12 blades.

Looking at the diffuser results, it is interesting to notice that the pressure recovery coefficient for the baseline and improved geometries, both in the 1D and 3D analysis, were very similar. This behavior can be due to the fact that the improvement done aimed for a higher efficiency, and, as seen in the sensitivity analysis, the diffuser variable has low impact in the isentropic efficiency, especially when compared to the impeller geometry.

A qualitative view of the geometric changes between the baseline and improved geometries can be seen in Figure (7) below.

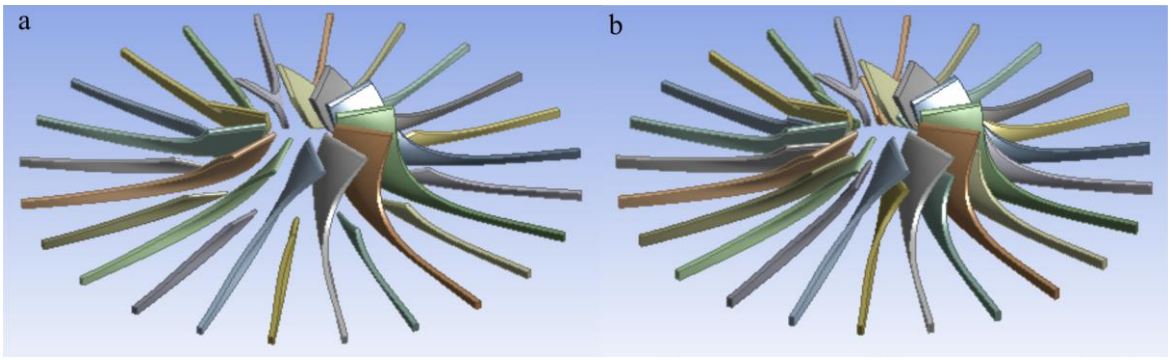

Figure 7. Baseline (a) and improved (b) 3D geometries.

The CFD simulation also provides a good way to analyze what is causing the increase in efficiency, Figures (8) and (9) show the fluid velocity in a plane located at 10% of the channel height away from the shroud for the baseline and optimized geometries.

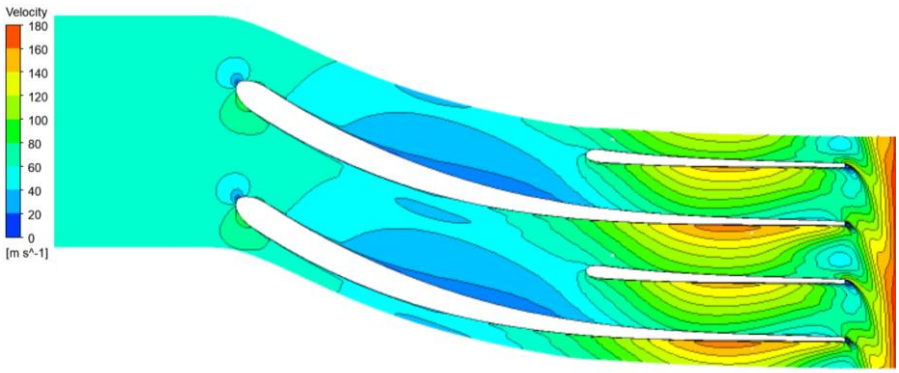

Figure 8. Baseline geometry velocity contour.

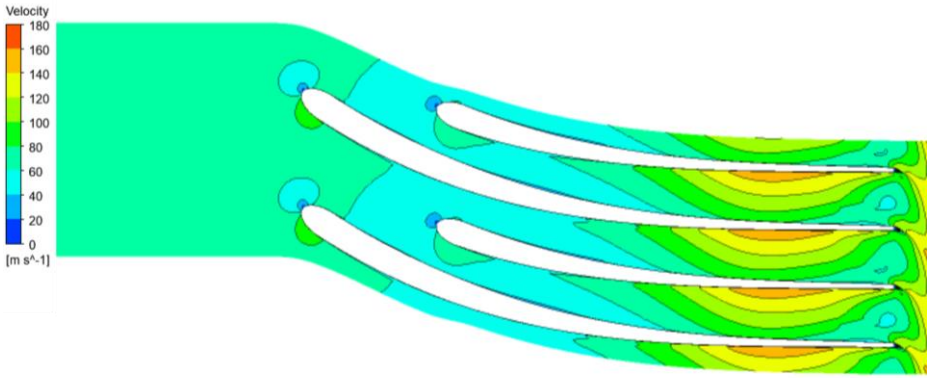

Figure 9. Improved geometry velocity contour.

Through the images it's possible to see that the improved geometry provides a smaller blockage at the impeller trailing-edge, along with that, the low velocity zone seen in Figure (8) between the blade and splitter leading edges is greatly reduced. This second phenomenon shows the importance of the splitter length, that breaks the growth of said zone, better guiding the fluid flow.

4. ACKNOWLEDGEMENTS

This work was supported by the National Agency of Petroleum, Natural Gas and Biofuels (ANP) and Shell Brazil Ltda., through the investment in Research, Development and Innovation Clause, contained in contracts for Exploration, Development, and Production of Oil and Natural Gas.

5. REFERENCES

Ameli A, Afzalifar A, Turunen-Saaresti T, Backman J., 2019. Centrifugal compressor design for near-critical point applications. J Eng Gas Turbines Power 141:. https://doi.org/10.1115/1.4040691.

Aungier R.H., 2000. Centrifugal Compressors - A Strategy for Aerodynamic Design and Analysis. ASME PRESS, New York.

Balje OE, 1981. Aerodynamic and Geometric Design Criteria for the Performance of Low Powered Vehicular Gas Turbines. Gas Turbine Power 103:158–167.

Brenes B.M., 2014a. Design of supercritical carbon dioxide centrifugal compressors. Universidad de Sevilla, Sevilla.

Brenes B.M., Sánchez D, Savill M, et al (2014b) A Design Strategy for Supercritical CO2 Compressors. In: ASME Turbo Expo 2014. ASME, Dusseldorf, Germany.

Campolongo F, Cariboni J, Saltelli A, 2007. An effective screening design for sensitivity analysis of large models. Environ Model Softw 22:1509–518. https://doi.org/10.1016/j.envsoft.2006.10.004.

Ge Q, Ciuffo B, Menendez M (2014) Combining screening and metamodel-based methods: an efficient sequential approach for the sensitivity analysis of model outputs. Reliab Eng Syst Saf 134:334– 344. https://doi.org/10.1016/j.ress.2014.08.009

Khan C., Amin R., Madden G., 2013.Carbon dioxide injection for enhanced gas recovery and storage (reservoir simulation), Egyptian Journal of Petroleum,Volume 22, Issue 2,Pages 225-240,ISSN 1110-0621, https://doi.org/10.1016/j.ejpe.2013.06.002.

Loewenthal H, 1984. Design of Power-Transmitting Shafts. Lewis Research Center, Cleveland, Ohio. NASA reference publication 1123.

McLeroy, P.G., Riva, Joseph P., Atwater, Gordon I., 2019. "Petroleum". Encyclopedia Britannica, 12 Aug. 2019, https://www.britannica.com/science/petroleum.

Morris M.D., 1991. Factorial sampling plans for preliminary computational experiments. Technometrics 33:161–174. https://doi.org/10.1177/001872086700900503.

NETL, 2010. Carbon Dioxide Enhanced Oil Recovery, National Energy Technology Laboratory NETL, U.S Department of Energy, USA. https://netl.doe.gov/oil-gas/oil-recovery

Oh HW, Yoon ES, Chung MK, 1997. An optimum set of loss models for performance prediction of centrifugal compressors. In: Proceedings of the Institution of Mechanical Engineers, Part A: Journal of Power and Energy. pp 331–338.

R.Span, W.Wagner, 1994. A New Equation of State for Carbon Dioxide Covering the Fluid Region from the Triple-Point Temperature to 1100 K Pressures up to 800 MPa. J Chem 25:

Saltelli A, Ratto M, Andres T et al, 2008. Global sensitivity analysis. The Primer. John Wiley & Sons Ltd, Chichester

Schlichting H, 1979. Boundary Layer Theory, Seventh Ed.

Stanitz J.D., 1952. One-dimensional compressible flow in vaneless diffusers of radial- and mixed-flow centrifugal compressors, including effects of friction, heat transfer and area change. Cleveland, Ohio. NACA TN 2610.

Vanrolleghem PA, Mannina G, Cosenza A, Neumann MB (2015) Global sensitivity analysis for urban water quality modelling: terminology, convergence and comparison of different methods. J Hydrol 522: 339–352. https://doi.org/10.1016/j.jhydrol.2014.12.056

Wiesner FJ, 1967. A Review of Slip Factors for Centrifugal Impellers. J Eng Power 89:558–566. https://doi.org/10.1115/1.3616734.

Wright S., Radel R., Vernon M., Rochau G., Pickard P., 2010. Operation and Analysis of a Supercritical CO_2 Brayton Cycle. Sandia National Laboratories, Albuquerque, New Mexico. SANDIA REPORT SAND2010-0171.

6. RESPONSIBILITY NOTICE

The authors are the only responsible for the printed material included in this paper.